Urbanisation increases cloudiness over Greater Kuala Lumpur during southwest and northeast monsoons

Sharifah Faridah Syed Mahbar[1,2] and Hiroyuki Kusaka[3]

[1] *Graduate School of Life and Environmental Sciences, University of Tsukuba, Tsukuba, Japan*
[2] *Malaysian Meteorological Department, Petaling Jaya, Malaysia*
[3] *Center for Computational Sciences, University of Tsukuba, Tsukuba, Japan*

Introduction

The impact of urbanisation on cloud formation is an ongoing and intriguing subject of debate. Studies on the urban heat island (UHI) effect are well documented for understanding urban–rural contrasts (Oke, 1973; Klysik and Fortuniak, 1999; Kusaka, Kimura, *et al*., 2000; Kusaka, Chen, *et al*., 2012; Morris, Chan, *et al*., 2016; Ramakreshnan, Aghamohammadi, *et al*., 2018; Vitanova and Kusaka, 2018) and urban precipitation has been extensively studied (Fujibe, Togawa, *et al*., 2009; Niyogi, Pyle, *et al*., 2011; Miao, Chen, *et al*., 2011; Kusaka, Nawata, *et al*., 2014; Kusaka, Nishi, *et al*., 2019; Li, Fowler, *et al*., 2020; Doan, Kobayashi, *et al*., 2023; Ghielmini, Pausata, *et al*., 2024). Nevertheless, little is known about how clouds form in urban areas (Theeuwes, Boutle, *et al*., 2021). While some statistical studies on cloud occurrence using satellite data (e.g. Rabin and Martin, 1996; Romanov, 1999; Theeuwes, Barlow, *et al*., 2019), show that clouds form more in cities than in rural areas, the topic remains ambiguous, particularly in cities in the Southeast Asia (SEA) region, which have not been investigated at all. Given the rapid population growth in cities globally (Haimeng, Fang, *et al*., 2018), there is a significant need to investigate the impact of cities on cloud occurrence, which could benefit urban dwellers both now and in the future.

Clouds play a crucial role in regulating the Earth's heat budget and global hydrological cycles (Yang, Zhao, *et al*., 2020). They act as shields that reflect incoming sunlight, contributing to planetary cooling, as well as blankets that trap outgoing radiation, which helps maintain atmospheric temperature (Trenberth and Fasullo, 2009; Betts, Desjardins, *et al*., 2013; Diaz, Gonzalez, *et al*., 2015; Harrop and Hartmann, 2016; Kebiao, Yuan, *et al*., 2019). Additionally, clouds modulate atmospheric conditions and increase the likelihood of precipitation (McLeod, Shepherd, *et al*., 2024). These interactions highlight the complex relationships between clouds and the atmospheric system. Changes in local cloud patterns in urban areas can disrupt energy and water cycles, leading to urban hazards (Vo, Hu, *et al*., 2023). Studies have been conducted to better understand the uncertainties and behaviour of cloud formation, particularly in urbanised areas. For example, Landsberg (1981) focused on New York City, Romanov (1999) on Moscow, Kanda, Inoue, *et al*. (2001) on Tokyo, Inoue and Kimura (2007) further studied Tokyo, and Theeuwes, Barlow, *et al*. (2019) on Paris and London. Romanov (1999) estimated the urban influence on cloud cover using satellite data for the Moscow region; the study analysed two seasons, representing the highest and lowest cloud cover differences. It was determined that cloudiness in urban areas is prominent during spring and summer compared to winter owing to the instability of the atmosphere, which influences the advection process that promotes cloud formation and distribution. Inoue and Kimura (2007) conducted numerical experiments during clear, calm summer days and showed that the cloud fraction and sensible heat distribution over urban areas were higher than those in rural environments. The model also revealed that small cumulus clouds were more prevalent in urban areas, but less common in suburbs and rural areas.

Other urban climate-related studies have found that the relative humidity is lower near urban surfaces (Moriwaki, Watanabe, *et al*., 2013; Yang, Ren, *et al*., 2017) and that the number of fog days has decreased over time, with urban fog formations almost non-existent (Akimoto and Kusaka, 2015). Instead, cloud cover has increased over urbanised areas and higher cloud-based levels (CBL) have been discovered due to excessive heat release over these areas (Romanov, 1999; Moriwaki, Watanabe, *et al*., 2013). Kang and Bryan (2011) also found that the CBL height over warmer surfaces increased with the amplitude of surface heterogeneity. Furthermore, Quante (2004) extensively discussed the global occurrence of clouds, which is highly dependent on geographical location, albedo, surface temperature, seasonality and time.

Taking advantage of high temporal and spatial resolution observations from the Himawari-8 satellite, our study investigated the impact of urbanisation on the distribution and frequency of cloud cover in the Greater Kuala Lumpur (GKL) area, the most densely urbanised conurbation in Malaysia (Ooi, Chan, *et al*., 2017). The Himawari-8 dataset is commonly used to assess cloud dynamics on a meso-micro scale, monitor weather patterns and predictions, detect extreme weather systems and analyse the impacts of urbanisation on local climates (e.g. Honda *et al*., 2018; Yang, Zhao, *et al*., 2020; Jumianti *et al*., 2024). Its proven reliability makes it particularly well-suited for the current study. The GKL is located on the west coast of Peninsular Malaysia and is bounded by the Straits of Malacca to the west and the Titiwangsa Mountain range to the east. The Asian-Australian monsoon and prevailing winds have a significant influence on regional weather patterns (Tangang, Farzanmanesh, *et al*., 2017; Jamaluddin, Tangang, *et al*., 2018). From June to August, southwesterly winds prevail in the region, which is known as the southwest monsoon (dry season, JJA), while northeasterly winds prevail from December to February, characterising the northeast monsoon (wet season, DJF).

To the best of our knowledge, this study is the first statistical analysis to investigate the impact of urbanisation on the presence of urban clouds in SEA. Our analysis focuses on these two main seasons in Malaysia, JJA and DJF, and covers the period 2016–2021. The main objectives of this study are as follows:

- Identify urbanisation effect in cloud cover distribution and frequency in GKL;
- Investigate the diurnal and periodic changes in cloud cover over GKL and rural surroundings;
- Evaluate how clouds affect surface temperature and relative humidity in GKL.

Data and methodology

Datasets

Himawari-8 is a new generation geostationary satellite equipped with an Advanced Himawari Imager (AHI), which is the most advanced sensor on board (Yamamoto, Ishikawa, *et al*., 2018). The operational phase of the Himawari-8 satellite commenced in July 2015, followed by backup operation of the Himawari-9 satellite in March 2017. Both satellites are slated to conduct observations until approximately 2029, under the Japan Meteorological Agency (JMA). AHI on board Himawari-8/9 are greatly improved over the previous MTSAT (Multifunctional Transport Satellite) series, with an increase in observation bands from 5 to 16. The spatial resolution is higher, ranging from 0.5 to 2km for the visible (VIS) band and 2km for the near-infrared (NIR) and infrared (IR) bands, while the temporal resolution has been enhanced to between 2.5 and 10min (Bessho *et al*., 2016).

In this study, a cloud mask dataset was created utilising land surface temperature (AHILST) cloud mask data obtained from the Himawari-8 satellite covering the study period from 2016 to 2021. The cloud mask algorithm employed is based on the methodology outlined by Yamamoto, Ishikawa, *et al*. (2018) to calculate the cloud mask from multi-wavelength data. These data are represented by binary values, where '0' indicates the absence of clouds ('no cloud') and '1' indicates the presence of clouds ('cloud'). To visualise the land use and land cover (LULC) in the GKL and surrounding areas, LULC data derived from ESA Sentinel-2 imagery with a 10m resolution were used. This product, produced using a deep learning model, categorises LULC into nine classes: water, trees, flooded vegetation, crops, built-up areas, bare ground, snow/ice, clouds and rangelands (Karra, Kontgis, *et al*., 2021), as illustrated in Figure 1.

Statistical method and analysis

Initially, we randomly selected several images of cloud cover over the GKL on hot and sunny days for visualisation analysis, as shown in Figure 2. These images consistently show a higher concentration of cloud formation over the centre of the GKL than over the surrounding rural areas. To determine whether these occurrences were isolated cases, we applied an 80th percentile assessment method to hourly temperature data from 2016 to 2021 to identify hot days. This analysis was conducted separately for each season (JJA and DJF) using data from four rural stations: Jalan Acob (JA), Kalumpang (KAL), Sg. Buloh (SBL) and Tennamaran Estate (TEN) (see Figure 1), which served as control environments. The datasets were arranged in ascending order and the respective value at the 80th percentile was defined as the hot days' threshold, which was then used to examine the cloud cover distribution during these specific events. The percentile method is commonly used in climate and weather studies to identify extreme events or anomalies within a dataset (e.g. Loon, Van Huijgevoort, *et al*., 2012; Russo *et al*., 2014; Wang *et al*., 2022). In addition, only days without daytime precipitation were considered to ensure that the analysis effectively highlighted the urban–rural contrast in terms of cloud occurrence without interference from convective activity. The reference hour for extracting these cases was set to 1500 local time (LT), a period typically characterised by the highest temperatures in both seasons, as shown in Figure S1. The methodological details and flow of analysis in this study are summarised in Figure S2.

The next step involved estimating the distribution of cloud cover on the selected dates. Using the AHILST cloud mask data from the Himawari-8 satellite, we applied an accumulation method to count the frequency of cloud days, followed by subsequent diurnal and seasonal averaging relative to the total number of hot days. A 'cloud day' is defined as any day when the cloud mask data from the Himawari-8 satellite indicates the presence of clouds, represented by a value of '1' (see Section 'Datasets'). In addition, to assess the accuracy of the cloud amount estimation

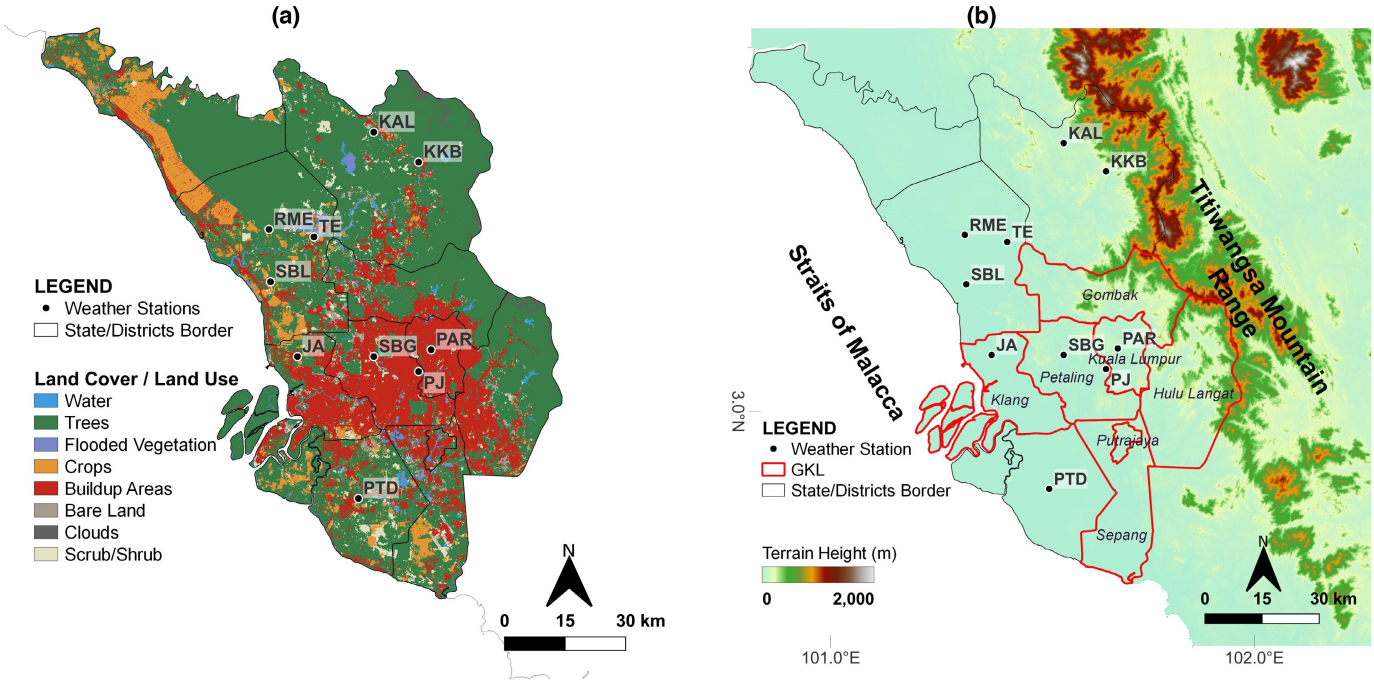

Figure 1. (a) ESA Sentinel-2 imagery at a 10m resolution from 2017, used to identify and categorise the reference stations in this study. Parlimen (PAR), Petaling Jaya (PJ) and Subang (SBG) are referred to as built-up areas and categorised as urban stations, while Jalan Acob (JA), Kalumpang (KAL), Kuala Kubu Baru (KKB), Pertanian Telok Datok (PTD), Raja Musa Estate (RME), Sg. Buloh (SBL) and Tennamaran Estate (TE) are categorised as trees/crops land cover and grouped as rural stations. (b) Terrain height of the study area. Red lines and black lines mark the GKL area and the districts' administrative borders, respectively. Black dots indicate the locations of weather stations for reference and analysis.

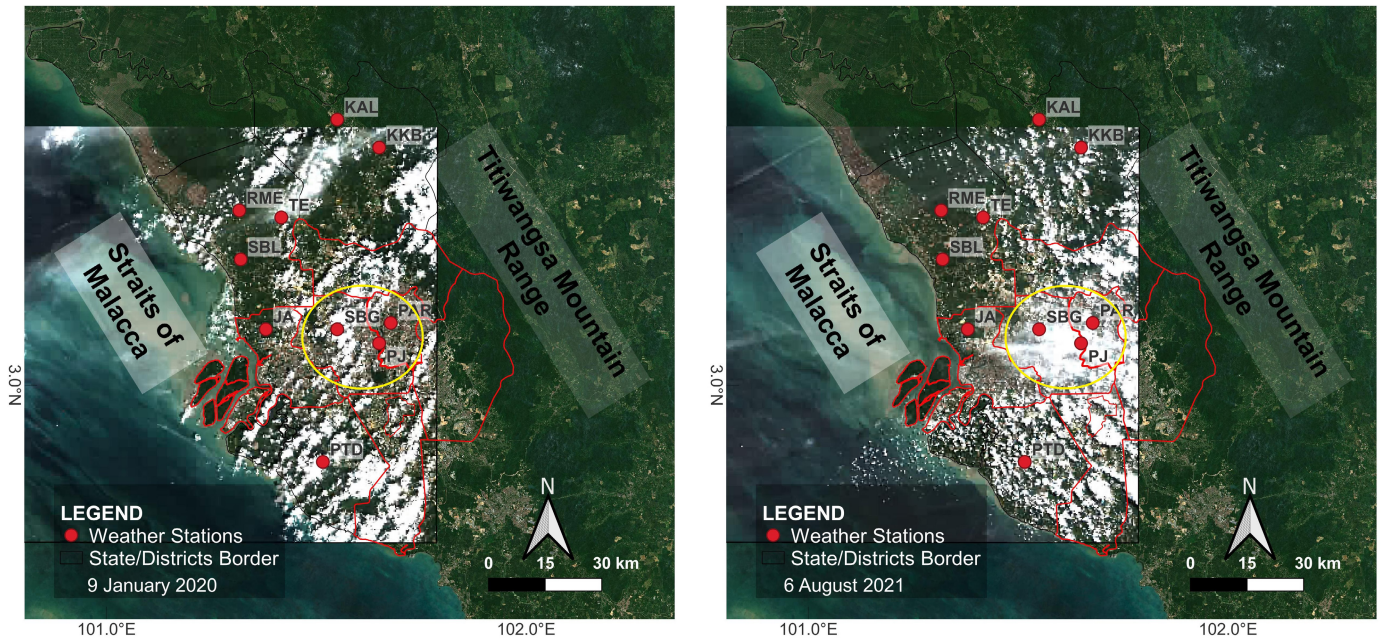

Figure 2. Cloud cover distribution during hot days in GKL. Image from Sentinel-2 products displayed in QGIS version 3.22.8. (Source: https://scihub.copernicus.eu/apihub). Yellow circles indicate the centre of GKL, where dense cloud formation is evident. Due to limitations in width and height parameters on some WMS servers (e.g. UMN MapServer), the WMS layer will not be printed. Left panel: case on 9 January 2020; right panel: case on 6 August 2021.

derived from satellite data, we compared observations from two meteorological stations within the study area. Stations PJ and SBG, which are categorised as urban sites, were the only stations in the study area that recorded cloud cover data.

We used the Himawari-8 land surface temperature (LST) dataset to estimate surface temperature variability during the study period. This allowed us to ascertain the spatial and temporal distributions of surface temperature in the presence of clouds in urban areas. We also used surface temperature and relative humidity data from observation stations to determine and compare diurnal patterns and seasonal changes in the parameters due to cloudiness.

Results

The 80th percentile assessment of hourly temperature data from 2016 to 2021 identified 141 hot day cases with a threshold of 33.2°C during JJA and 227 cases with a threshold of 32.9°C during DJF. Figure 3 clearly shows the disparity in cloud cover distribution across the seasons, with DJF having a higher number of cloudy days than JJA. In urban areas, the number of cloudy days recorded at 1500 LT during JJA ranged from 90 to 121 days, out of a total of 141 cases. For DJF, cloudy days in urban areas ranged from 131 to 187 days, out of 227 cases. In contrast, fewer cloudy days were observed in rural areas, ranging between 78 and 95 days during JJA and 102 and 164 days during DJF.

Table 1 compares the ratios at 1000 LT, 1500 LT and 1800 LT between urban and rural cloudy days. The data clearly show that there were more cloudy days in urban areas than in rural areas, with the maximum average peak at 1500 LT being 1.22 times higher in JJA and 1.24 times higher in DJF. Furthermore, the assessment of daytime cloudiness frequency by month for each

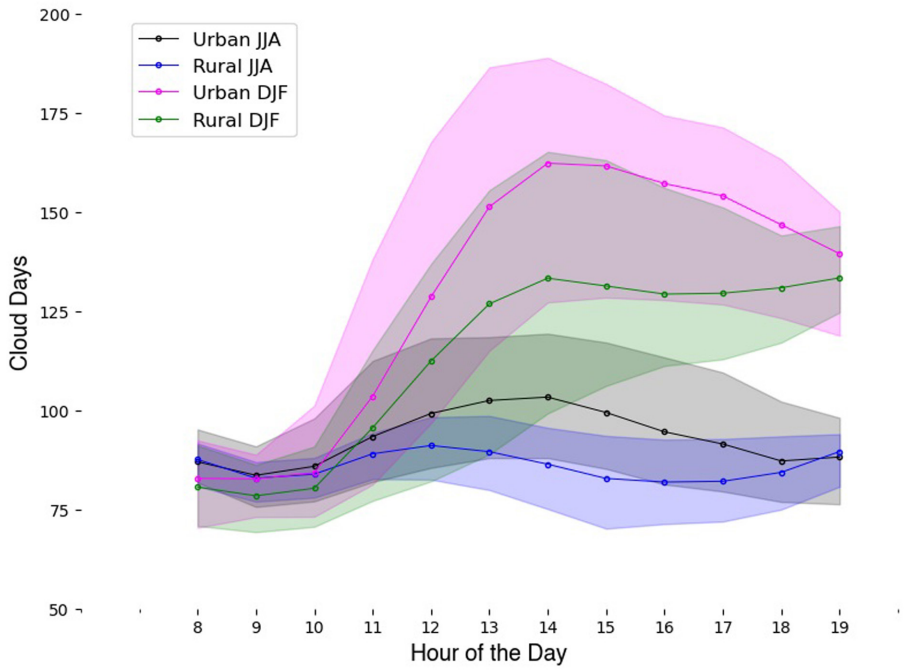

Figure 3. Daytime cloud coverage on hot days during the southwest monsoon (dry season, JJA) and northeast monsoon (wet season, DJF) for the period of 2016–2021. The differences in cloud distribution between urban and rural areas are clear, as is the distinction between seasons. The DJF season sees more cloud formation than JJA.

Table 1

Ratio analysis of urban cloud days to rural cloud days.

Period	*1000 LT*	*1500 LT*	*1800 LT*
JJA	82/81 ≈ 1.01	105/86 ≈ 1.22	91/86 ≈ 1.06
DJF	83/82 ≈ 1.01	163/131 ≈ 1.24	148/132 ≈ 1.12

season during hot days, estimated from surface observation stations and satellite data, yielded smaller root mean squared error (RMSE) values with minimal percentage errors of 7% and 5% for PJ in JJA and DJF, respectively, and 3% and 6% for SBG in JJA and DJF, respectively (Figure 4). This confirms that the satellite data used in this study are compatible with data from surface observation stations.

As the day progressed, the clouds increased in tandem with the rising daytime temperatures. Cloud cover peaked between 1400 LT and 1600 LT, before gradually decreasing (Figure 3), mirroring the temperature pattern. This pattern of cloud formation and dissipation is influenced by surface and near-surface UHI effects, resulting in dramatic differences in cloud distribution between urban and rural areas. According to Wallace (1975), the diurnal cloud cycle, driven by convective cloud formation, is closely related to the thermodynamic response of the diurnal cycle of LST (Chepfer, Brogniez, *et al*., 2019).

Figure 5 shows the diurnal profiles of the near-surface temperature and relative humidity used to assess the sensitivity of the surface parameters to clouds. During JJA, the near-surface temperatures in urban areas peak at 33.3°C (1600 LT) and drop to 26.1°C (0700 LT). In rural areas, near-surface temperatures peak at 33.0°C (1500 LT) and drop to 24.2°C (0700 LT). In DJF, near-surface temperatures over urban areas average at 33.4°C (1500 LT), with a minimum of 25.5°C (0700 LT). In rural areas, average near-surface temperatures peak at 32.5°C (1500 LT) with a minimum of 23.5°C (0700 LT). During the JJA, the surface relative humidity in urban areas ranged from 52% (1500 LT) to 83% (0600 LT), whereas that in rural areas ranged from 52% (1500 LT) to 92% (0700 LT). During DJF, the relative humidity observed in urban areas ranged from 49% (1300 LT) to 85% (0600 LT), while that in rural areas ranged from 58% (1400 LT) to 94% (0800 LT). The urban–rural contrast was clearly pronounced in both seasons, with urban areas exhibiting warmer temperatures and lower humidity than rural areas.

Figure 6 illustrates the spatial distribution of the total cloud days and average LST calculated from Himawari-8 satellite datasets. In addition to the typical cloud formation over mountainous regions, which can be attributed to orographic uplift and convection processes, the centre of the GKL consistently had more cloudy days than the surrounding rural areas, regardless of season. However, there were more cloudy

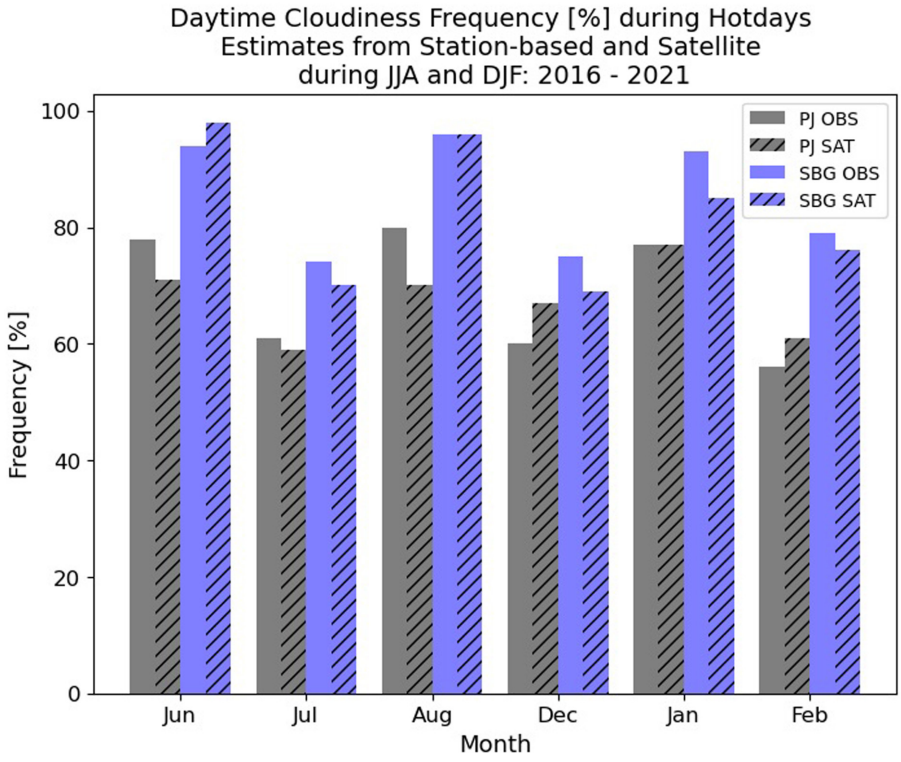

Figure 4. Comparison of daytime cloudiness frequency (in percentage) during hot days, estimated from surface meteorological observation stations and Himawari-8 datasets. The analysis covers the study period from 2016 to 2021, focusing on hot days cases, during the JJA and DJF seasons.

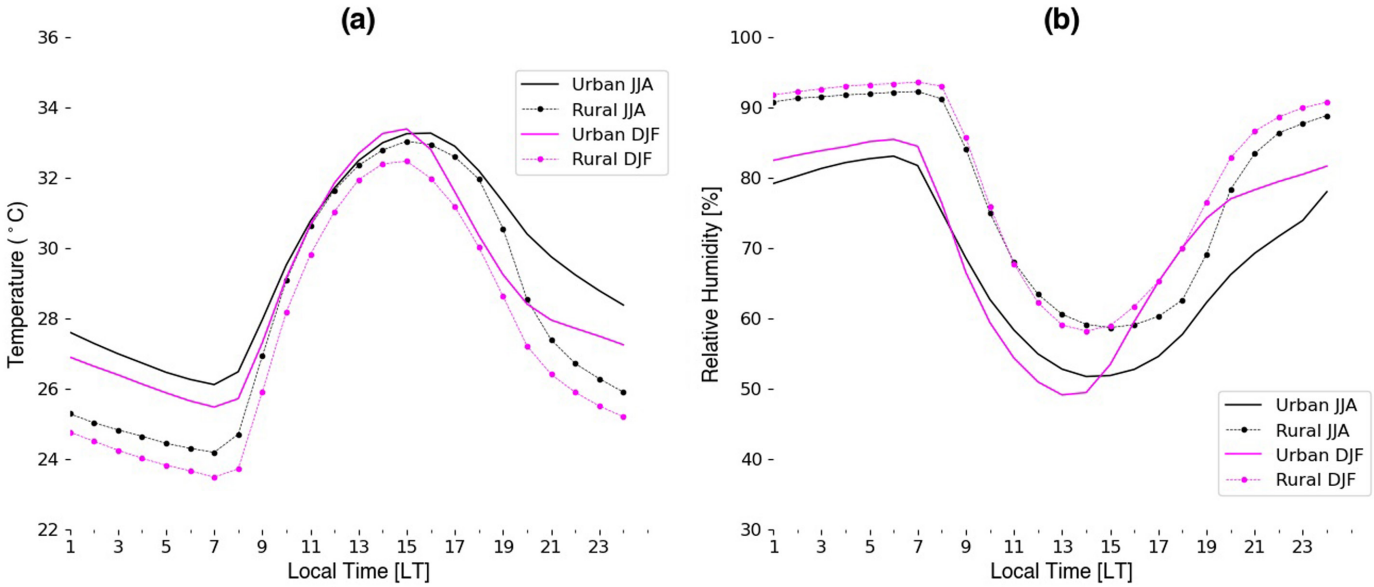

Figure 5. (a) Diurnal profiles of 2m temperature on hot days during JJA and DJF for the period of 2016–2021. (b) Diurnal profiles of 2m relative humidity over the same period. Both profiles highlight significant differences between urban and rural environments, with urban areas showing higher temperatures and lower humidity. The contrasts between JJA and DJF are more pronounced in the nocturnal profiles for both parameters.

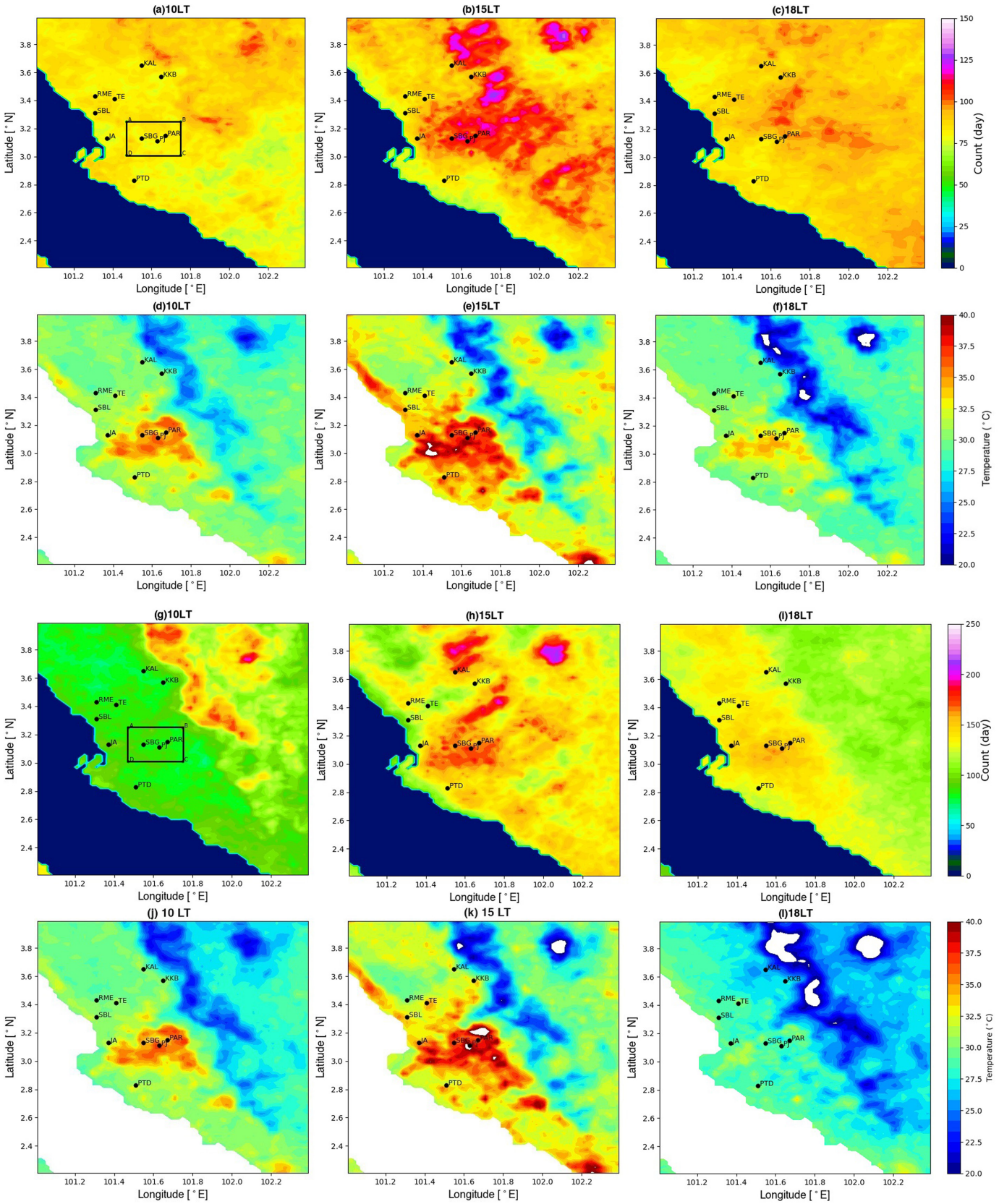

FIGURE 6. (a–c) Shows the number of clouds (days) at 1000 LT, 1500 LT and 1800 LT from satellite datasets. (d–f) Average land surface temperatures (LST) at 1000 LT, 1500 LT and 1800 LT from satellite datasets. The distribution was based on the JJA season. The black square represents the area where the spatially averaged computation for the urban site was conducted. (g–i) Shows the number of clouds (days) at 1000 LT, 1500 LT and 1800 LT from satellite datasets. (j–l) Average land surface temperature (LST) at 1000 LT, 1500 LT and 1800 LT from the satellite datasets. Distribution was observed during the DJF season. The black square represents the area where the spatially averaged computation for the urban site was conducted.

days during DJF than in JJA. Excessive heat is evident over the GKL, with a noticeable increase in temperature at around 1500 LT. During this period, the cloud coverage clearly extends westward into the Klang district (see Figure 1), which is also part of the urbanised GKL region. In parallel, the LST rises in these areas, reaching 40.3°C during JJA and 41.8°C during DJF.

Discussion

The results discussed in the previous section clearly show that clouds form more frequently in urban areas than in rural areas. For instance, the ratio of urban to rural cloud days was consistently greater than 1, indicating more cloud cover in urban areas. The most pronounced ratio occurs between 1500 LT and 1800 LT. Figure 7 shows that higher global solar radiation or incoming shortwave radiation received between 1300 LT and 1500 LT at approximately 831.9W/m^2 during JJA and 821.4W/m^2 during DJF increases daytime temperatures, peaking at 1500 LT to 1600 LT (Figure 6). Betts, Desjardins, *et al*. (2013) found that this behaviour was caused by the diurnal cycle of incoming solar radiation. Trenberth and Fasullo (2009) discussed in detail about how feedback mechanisms in cloud cover relate to the amount of solar radiation reaching the surface. These diurnal variations directly influenced the increase and decrease in cloud cover. In urban areas, this process is exacerbated by UHI effects. According to Oke (1987), excessive heat release causes an increase in air temperature over urban areas that can extend vertically hundreds of meters (Romanov, 1999). This rise in condensation levels, combined with increased surface-heterogeneity amplitude over warmer surfaces, raises the CBL height (Romanov, 1999; Kang and Bryan, 2011; Moriwaki, Watanabe, *et al*., 2013). This process is thought to intensify convection and moist air lifting, resulting in increased cloud formation over urban areas and a widening of the cloud cover gap between urban and rural areas from 1500 LT to 1800 LT (see Figure 3).

In terms of seasonality, DJF had more cases of hot days (~42%) and higher cloudiness than JJA (~26%) over 6 years. Although DJF is typically associated with Malaysia's rainy season, this is not the case for GKL. As the region approaches the end of the rainy season, the west coast of Peninsular Malaysia, including the GKL, become drier. For example, February and March are considered to be the hottest months in Kuala Lumpur (Elsayed, 2012). According to Romanov (1999), warmer temperatures increase convection activity; so, cities have more clouds during the day than rural hinterlands. This is consistent with the cloud distribution results from JJA and DJF in both urban and rural areas (Figure 3). Furthermore, Theeuwes, Boutle, *et al*. (2021) found that urban-induced local circulation directs moist air towards city centres, promoting upward moisture convergence and increasing cloud formation, especially at low wind speeds.

In addition to the extensive cloud formation in the GKL areas, the relative humidity near the urban surfaces was lower than that in the surrounding rural areas, which is consistent with the findings of Yang, Ren, *et al*. (2017) for Beijing City and Moriwaki, Watanabe, *et al*. (2013) for the Matsuyama Plain. Moriwaki, Watanabe, *et al*. (2013) further investigated the diurnal and seasonal changes in absolute humidity between urban and rural areas by examining the urban dry island (UDI) phenomenon. The study discovered significant discrepancies in latent heat fluxes, with urban areas producing much lower latent heat fluxes than their rural counterparts, amplifying the UDI intensity. The intensity of the UDI was higher during summer and lower during winter, altering the cloud base levels in both urban and rural environments.

Based on our findings, the interaction of solar radiation, surface temperature and humidity drives the differences in cloud formation between urban and rural areas. In the GKL context, during cases for hot days, higher daytime solar radiation leads to substantial increases in urban surface temperature compared to the surrounding rural environments, as observed in Figure 5. The higher urban surface temperature contributes to higher sensible heat flux in urban environments, intensifying convection and promoting the lifting of moist air, which results in enhanced cloud formation in GKL. Conversely, the opposite conditions in rural areas maintain higher latent heat fluxes, leading to cooling through evapotranspiration and suppressing the cloud formation processes. According to Magnaye and Kusaka (2024), higher thermal inertia in urban environments leads to differences in sensible heat and latent heat fluxes. The UHI effect in GKL further amplifies these distinctions.

However, several studies (e.g. Vo, Hu, *et al*., 2023) have explored the feedback interaction of daytime urban cloud formation, which can impact the energy balance by reducing the amount of downward solar radiation reaching the surface. This reduction in solar radiation can moderate surface temperatures to some extent, counteracting some of the warming effects. Consequently, the existing urban–rural surface heating contrast may decrease. For a more comprehensive understanding of this feedback mechanism, particularly in tropical climate cities, further research using numerical weather forecasting models should be conducted.

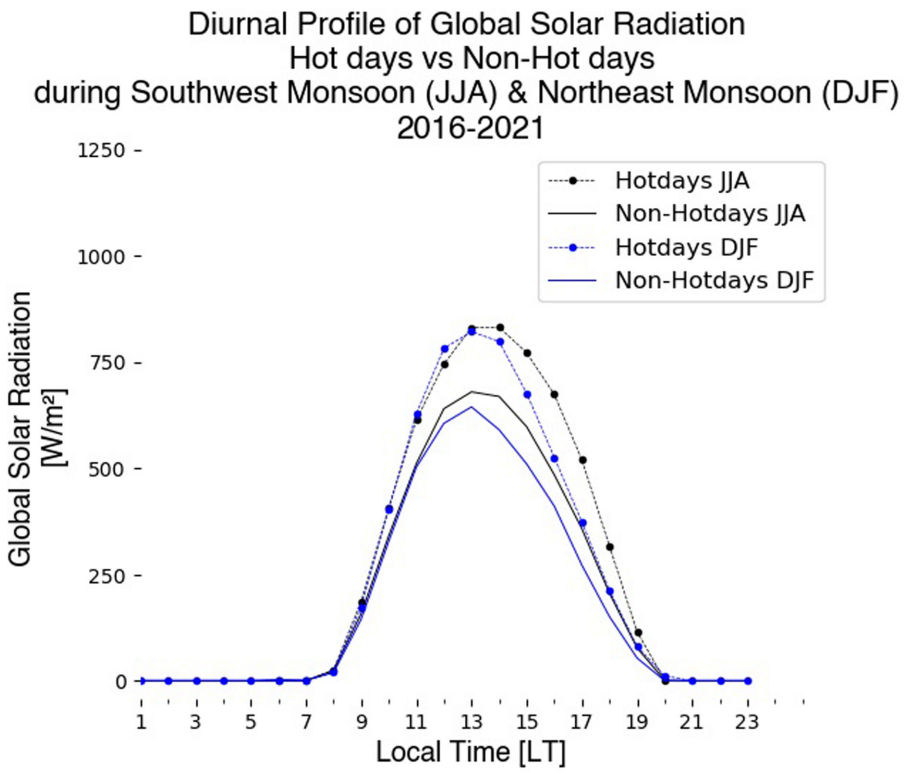

Figure 7. Diurnal profiles of global solar radiation during hot days compared to non-hot days in the JJA and DJF seasons, respectively. During JJA, the solar radiation on hot days reached 831.9W/m^2 compared to 679.9W/m^2 on non-hot days. During DJF, the solar radiation on hot days reached 821.4W/m^2, compared to 644.5W/m^2 on non-hot days.

Conclusion and remarks

Our study highlighted that despite GKL being part of the maritime continent, bound within the tropical climate region and known for its dense cloud cover and sparse clear-sky observations compared to mid-latitudes, the difference between urban and rural cloud cover is still stark and clearly distinguishable. The Himawari-8

satellite-based observations used in this study demonstrate robustness in contrasting cloud amounts over different surfaces. The influence of urban areas on cloudiness was most pronounced during DJF, experiencing approximately 1.24 times more cloudy days than rural areas at 1500 LT. This elevated ratio persisted until 1800 LT, when it decreased slightly to 1.12. During JJA, the ratio of urban to rural cloudy days is 1.22 around 1500 LT and 1.06 around 1800 LT. Cloudiness is relatively high between 1400 LT and 1500 LT in both seasons, which is related to increased solar radiation that raises surface temperatures and amplifies the UHI effects, thus promoting cloud formation. Our study concluded that in the GKL area, cloud cover predominates with warmer temperatures and relatively drier humidity. In contrast, rural areas with cooler temperatures and higher humidity experienced less cloud formation.

Our study provides valuable insights into the current state of knowledge about cloud formation in tropical cities, especially in SEA countries, which is relevant to broader global climate change issues related to rapid urbanisation. We believe that the findings of this study contribute to the better understanding of the mechanisms of urban cloud enhancement, particularly under different seasonal and diurnal conditions in various regions with varying climatic characteristics. These results highlight the significant impact of urbanisation on local weather patterns and contribute to improved climate models and urban planning strategies.

Additionally, we believe that our findings can help the local government in improving current climate change policies, particularly those aimed at urban sustainability. This will help refine roadmaps and align them with the latest research. However, it is worth noting that our study did not investigate the role of aerosols in urban environments despite their significant influence on cloud formation and precipitation processes. Future research should incorporate comprehensive climatological and numerical analyses to deepen our understanding and generate robust data. This approach will advance our understanding of urban climate dynamics and help develop effective strategies to mitigate the impact of rapid urbanisation on both local and global climates.

Acknowledgements

This study was supported by JSPS KAKENHI (grant numbers JP24K07130 and JP23H05494). We thank the Malaysian Meteorological Department (MET Malaysia) for providing the observational data used in our statistical analysis. We also thank our group member Nobuyasu Suzuki for his technical support in data preparation. The first author would like to express her gratitude to the Public Service Department of Malaysia for the scholarships.

Author contributions

Sharifah Faridah Syed Mahbar: Conceptualization; methodology; data curation; investigation; validation; formal analysis; visualization; writing – original draft. **Hiroyuki Kusaka:** Conceptualization; methodology; supervision; funding acquisition; project administration; resources; writing – review and editing.

Conflict of interest statement

The authors declare that they have no competing financial or non-financial interests that could influence the content or findings of this study.

Data availability statement

The data used in this study are available upon request. Some data are subject to provisions outlined in the Data Act, which preclude sharing.

Supporting Information

Additional supporting information may be found online in the Supporting Information section at the end of the article.
Figure S1

References

Akimoto Y, **Kusaka H**. 2015. A climatological study of fog in Japan based on event data. *Atmos. Res.* **151**: 200–211. https://doi.org/10.1016/j.atmosres.2014.04.003

Bessho K, **Date K**, **Hayashi M** *et al*. 2016. An introduction to Himawari-8/9 – Japan's new-generation geostationary meteorological satellites. *J. Meteorol. Soc. Jpn.* **94**(2): 151–183. https://doi.org/10.2151/jmsj.2016-009

Betts AK, **Desjardins R**, **Worth D**. 2013. Cloud radiative forcing on the diurnal cycle climate of the Canadian Prairies. *J. Geophys. Res. Atmos.* **118**: 8935–8953. https://doi.org/10.1002/jgrd.50593

Chepfer H, **Brogniez H**, **Noel V**. 2019. Diurnal variations of cloud and relative humidity profiles across the tropics. *Sci. Rep.* **9**: 16045. https://doi.org/10.1038/s41598-019-52437-6

Diaz JP, **Gonzalez A**, **Exposito FJ** *et al*. 2015. WRF multi-physics simulation of clouds in the African region. *Q. J. R. Meteorol. Soc.* **141**: 2737–2749. https://doi.org/10.1002/qj.2560

Doan Q-V, **Kobayashi S**, **Kusaka H** *et al*. 2023. Tracking urban footprint on extreme precipitation in an African Megacity. *J. Appl. Meteorol. Climatol.* **62**: 209–226. https://doi.org/10.1175/JAMC-D-22-0048.1

Elsayed ISM. 2012. Mitigation of the urban heat island of the city of Kuala Lumpur, Malaysia. *Middle-East J. Sci. Res.* **11**: 1602–1613. https://doi.org/10.5829/idosi.mejsr.2012.11.11.1590

Fujibe F, **Togawa H**, **Sakata M**. 2009. Long-term change and spatial anomaly of warm season afternoon precipitation in Tokyo. *Sola* **5**: 17–20. https://doi.org/10.2151/sola.2009-005

Ghielmini C, **Pausata FSR**, **Argueso D** *et al*. 2024. Evaluationg the role of city representation in modelling the urban precipitation effect of Kuala Lumpur. *Urban Clim.* **55**: 101907. https://doi.org/10.1016/j.uclim.2024.101907

Haimeng L, **Fang C**, **Miao Y** *et al*. 2018. Spatio-temporal evolution of population and urbanization in the countries along the Belt and Road 1950–2050. *J. Geogr. Sci* **28**(7): 919–936. https://doi.org/10.1007/s11442-018-1513-x

Harrop BE, **Hartmann DL**. 2016. The role of cloud radiative heating within the atmosphere on the high cloud amount and top-of-atmosphere cloud radiative effect. *J. Adv. Model. Earth Syst.* **8**: 1391–1410. https://doi.org/10.1002/2016MS000670

Honda T, **Miyoshi T**, **Lien GY** *et al*. 2018. Assimilating All-Sky Himawari-8 satellite infrared radiances: a case of Typhoon Soudelor (2015). *Mon. Weather Rev.* **146**: 213–229. https://doi.org/10.1175/MWR-D-16-0357.1

Inoue T, **Kimura F**. 2007. Numerical experiments on fair-weather clouds forming over the urban area in northern Tokyo. *Sola* **3**: 125–128. https://doi.org/10.2151/sola.2007-032

Jamaluddin AF, **Tangang F**, **Chung JX** *et al*. 2018. Investigating the mechanisms of diurnal rainfall variability over Peninsular Malaysia using non-hydrostatic regional climate model. *Meteorog. Atmos. Phys.* **130**: 611–633. https://doi.org/10.1007/s00703-017-0541-x

Jumianti N, **Marzuki M**, **Yusnaini H** *et al*. 2024. Prediction of extreme rain in Kototabang using Himawari-8 satellite based on differences in cloud brightness temperature. *Remote Sens. Appl. Soc. Environ.* **33**: 101102. https://doi.org/10.1016/j.rsase.2023.101102

Kanda M, **Inoue Y**, **Uno I**. 2001. Numerical study on cloud lines over an urban street in Tokyo. *Boundry-Layer Meteorol.* **98**: 251–273.

Kang S-L, **Bryan GH**. 2011. A Larg-Eddy simulation study of moist convection initiation over heterogeneous surface fluxes. *Mon. Weather Rev. Am. Meteorol. Soc.* **139**: 2901–2917. https://doi.org/10.1175/MWR-D-10-05037.1

Karra K, **Kontgis C**, **Statman-Weil Z** *et al*. 2021. Global land use/land cover with Sentinel-2 and deep learning, in 2021 IEEE International Geoscience and Remote Sensing Symposium IGARSS: Brussels, 11–16 July 2021, pp 4704–4707. https://doi.org/10.1109/IGARSS47720.2021.9553499.

Kebiao M, **Yuan Z**, **Zuo Z** *et al*. 2019. Changes in global cloud cover based on remote sensing data from 2003 to 2012. *Chin. Geogra. Sci* **29**(2): 306–315. https://doi.org/10.1007/s11769-019-1030-6

Klysik K, **Fortuniak K**. 1999. Temporal and spatial characteristics of urban heat Island of Lodz, Poland. *Atmos. Environ.* **33**: 3885–3895.

Kusaka H, **Chen F**, **Tewari M** *et al*. 2012. Numerical simulations of Urban Heat Island effect by the WRF Model with 4-km grid increment: an inter-comparison study between Urban Canopy Model and Slab Model. *J. Meteorol. Soc. Jpn.* **90B**: 33–45. https://doi.org/10.2151/jmsj.2012-B03

Kusaka H, **Kimura F**, **Hirakuchi H** *et al*. 2000. The effects of land-use alteration on the sea breeze and daytime heat Island in the Tokyo Metropolitan area. *J. Meteorol. Soc. Jpn.* **78**(4): 405–420.

Kusaka H, **Nawata K**, **Suzuki-Parker A** *et al*. 2014. Mechanism of precipitation increase with urbanization in Tokyo as revealed by ensemble climate simulations. *J. Appl. Meteorol. Climatol.* **53**: 824–839. https://doi.org/10.1175/JAMC-D-13-065.1

Kusaka H, **Nishi A**, **Mizunari M** *et al*. 2019. Urban impacts on spatiotemporal patterns of short-duration convective precipitation in as coastal city adjacent to a mountain. *Q. J. Roy. Meteor.* **145**: 2237–2254. https://doi.org/10.1002/qj.3555

Landsberg HE. 1981. The Urban Climate. International Geophysics Series, Volume **28**. Academic Press: New York.

Li Y, **Fowler HJ**, **Argueso D** *et al*. 2020. Strong intensification of hourly rainfall extremes by urbanization. *Geophys. Res. Lett.* **47**: e2020GL088758. https://doi.org/10.1029/2020GL088758

Loon AFV, **Van Huijgevoort MHJ**, **Van Lanen HAJ**. 2012. Evaluation of drought propagation in an ensemble mean of large-scale hydrological models. *Hydrol. Earth Syst. Sci.* **16**: 4057–4078. https://doi.org/10.5194/hess-16-4057-2012

Magnaye AMT, **Kusaka H**. 2024. Potential effect of urbanization on extreme heat events in Metro Manila Philippines using WRF-UCM. *Sustain. Cities Soc.* **10**: 105584. https://doi.org/10.1016/j.scs.2024.105584

McLeod J, **Shepherd M**, **Appelbaum M**. 2024. Evidence of cloud and rainfall modification in a mid-sized urban area – a climatological analysis of Augusta, Georgia. *City Environ. Interact.* **21**: 100141. https://doi.org/10.1016/j.cacint.2024.100141

Miao S, **Chen F**, **Li Q** *et al*. 2011. Impacts of urban processes and urbanization on summer precipitation: a case study of Heavy Rainfall in Beijing on 1 August 2006. *J. Appl. Meteorol. Climatol.* **50**: 806–825. https://doi.org/10.1175/2010JAMC2513.1

Moriwaki R, **Watanabe K**, **Morimoto K**. 2013. Urban dry Island phenomenon and its impact on cloud base level. *J. JSCE* **1**: 521–529.

Morris KI, **Chan A**, **Morris KJK** *et al*. 2017. Urbanisation and urban climate of a tropical conurbation, Klang Valley, Malaysia. *Urban Clim.* **19**: 54–71. https://doi.org/10.1016/j.uclim.2016.12.002

Niyogi D, **Pyle P**, **Lei M** *et al*. 2011. Urban modification of thunderstorms: an observational storm climatology and model case study for the indianapolis urban region. *J. Appl. Meteorol. Climatol.* **50**: 1129–1144. https://doi.org/10.1175/2010JAMC1836.1

Oke TR. 1973. City Size and the Urban Heat Island. *Atmos. Environ.* **7**: 769–779.

Oke TR. 1987. Boundary Layer Climates, 2nd Edition. Methuen Co: London, New York, pp 435.

Ooi MCG, **Chan A**, **Ashfold MJ** *et al*. 2017. Numerical study on effect of urban heating on local climate during calm intermonsoon period in greater Kuala Lumpur, Malaysia. *Urban Clim.* **20**: 228–250. https://doi.org/10.1016/j.uclim.2017.04.010

Quante M. 2004. The role of clouds in the climate system. *J. Phys. IV (Proceedings)* **121**: 61–86. https://doi.org/10.1051/jp4:2004121003

Rabin RM, **Martin DW**. 1996. Satellite observations of shallow cumulus coverage over the central United States: an exploration of land use impact on cloud cover. *J. Geophys. Res.* **101**: 7149–7155. https://doi.org/10.1029/95JD02891

Ramakreshnan L, **Aghamohammadi N**, **Fong CS** *et al*. 2018. Empirical study on temporal variations of canopy-level urban heat Island effect in the tropical city of Greater Kuala Lumpur. *Sustain. Cities Soc.* **44**: 748–762. https://doi.org/10.1016/j.scs.2018.10.039

Romanov P. 1999. Urban influence on cloud cover estimated from satellite data. *Atmos. Environ.* **33**: 4162–4172.

Russo S, **Dosio A**, **Graversen RG** *et al*. 2014. Magnitude of extreme heat waves in present climate and their projection in warming world. *J. Geophys. Res. Atmos.* **119**: 12500–12512. https://doi.org/10.1002/2014JD022098

Tangang F, **Farzanmanesh R**, **Mirzaei A** *et al*. 2017. Characteristics of precipitation extremes in Malaysia associated with El Nino and La Nina events. *Int. J. Climatol.* **37**: 696–716. https://doi.org/10.1002/joc.5032

Theeuwes NE, **Barlow JF**, **Teuling AJ** *et al*. 2019. Persistent cloud cover over mega-cities linked to surface heat release. *npj Clim. Atmos. Sci.* **2**: 15. https://doi.org/10.1038/s41612-019-0072-x

Theeuwes NE, **Boutle IA**, **Clark PA** *et al*. 2021. Understanding London's summertime cloud cover. *Q. J. R. Meteorol. Soc.* **148**: 454–465. https://doi.org/10.1002/qj.4214

Trenberth KE, **Fasullo JT**. 2009. Global warming due to increasing absorbed solar radiation. *Geophys. Res. Lett.* **36**: L07706. https://doi.org/10.1029/2009GL037527

Vitanova LL, **Kusaka H**. 2018. Study on the urban heat Island in Sofia City: numerical simulations with potential natural vegetation and present land use data. *Sustain. Cities Soc.* **40**: 110–125. https://doi.org/10.1016/j.scs.2018.03.012

Vo TT, **Hu L**, **Xue L** *et al*. 2023. Urban effects on local cloud patterns. PNAS Research Article. *Earth, Atmos. and Planet Sci.* **120**(21): e2216765120. https://doi.org/10.1073/pnas.2216765120

Wallace JM. 1975. Diurnal variations in precipitation and thunderstorm frequency over the conterminous United States. *Mon. Weather Rev.* **103**(5): 406–419. https://doi.org/10.1175/1520-0493(1975)103⟨0406:dvipat⟩2.0

Wang Y, **Xiang Y**, **Song L** *et al*. 2022. Quantifying the contribution of urbanization to summer extreme high-temperature events in the Beijing-Tianjin-Hebei urban agglomeration. *J. Appl. Meteorol. Climatol.* **61**: 669–683. https://doi.org/10.1175/JAMC-D-21-0201.1

Yamamoto Y, **Ishikawa H**, **Oku Y** *et al*. 2018. An algorithm for land surface temperature retrieval using three thermal infrared bands of Himawari-8. *J. Meteorol. Soc. Jpn* **96B**: 59–76. https://doi.org/10.2151/jmsj.2018-005

Yang P, **Ren G**, **Hou W**. 2017. Temporal-Spatial patterns of relative humidity and the Urban Dryness Island effect in Beijing City. *J. Appl. Meteorol. Climatol.* **56**: 2221–2237. https://doi.org/10.1175/JAMC-D-16-0338.1

Yang Y, **Zhao C**, **Fan H**. 2020. Spatiotemporal distributions of cloud properties over China based on Himawari-8 advanced Himawari imager data. *Atmos. Res.* **240**: 104927. https://doi.org/10.1016/j.atmosres.2020.104927

Correspondence to: H. Kusaka
kusaka@ccs.tsukuba.ac.jp

doi: 10.1002/wea.7644